Tribology and Materials
Vol. 4, No. 1, 2025, pp. 38-55

ISSN 2812-9717
https://doi.org/10.46793/tribomat.2025.005

Trends in corrosion resistance of electroless Ni-B-Mo coatings

Manik BARMAN [1,2], Tapan Kumar BARMAN [1], Prasanta SAHOO [1,*]

[1] Jadavpur University, Kolkata, India
[2] Heritage Institute of Technology, Kolkata, India
*Corresponding author: prasanta.sahoo@jadavpuruniversity.in

Keywords
electroless
bath composition
Ni-B-Mo
corrosion behaviour
EIS
PDP

History
Received: 21-10-2024
Revised: 20-01-2025
Accepted: 20-03-2025

Abstract

Ternary Ni-B-Mo coatings are prepared using various coating compositions through the chemical deposition method. AISI 1040 steel specimens are used as the substrate to develop coated layers. The chemical solution compositions are varied to understand their impact on coating behaviours. A three-electrode-based potentiostat is applied to determine corrosion behaviour. The experiments are carried out in a 3.5 wt. % NaCl solution. All the coated surfaces displayed a surface morphology resembling cauliflower. The coated layer thickness increased from 13 to 42 µm. The boron content increased with $NaBH_4$ concentration, resulting in an enhancement in corrosion behaviour. The electroless Ni-B coatings usually become rough, leading to corrosion resistance deterioration. While the molybdenum concentration does not significantly impact boron content, it deteriorates the corrosion resistance at its higher concentrations due to rougher surface morphology. The performance against corrosion at level 1 is worst due to cracked surface morphology, while the same performance is best at level 3 concentrations.

1. Introduction

AISI 1040 steel is commonly used in a range of industrial applications because of its superior mechanical properties, affordability and ease of manufacturing. However, one of the significant challenges associated with AISI 1040 steel is its susceptibility to corrosion under certain environmental conditions. Corrosion can significantly damage components, leading to structural weakness, loss of functionality and ultimately, economic losses. Hence, steel-made components are to be protected from corrosion. A different variant of coatings comes into play in such situations. Different types of coatings protect different base metals against various harsh environments from damage. These variants of coatings are usually applied through various techniques such as electrodeposition, PVD, CVD and electroless methods. In this context, electroless coatings can be applied on metal or non-metal substrates with complicated and sharp edges. Such advantages make the electroless coatings more favourable than other coating deposition techniques. Electroless Ni-B (ENB) coatings usually have very good physical, mechanical and tribological properties.

Electroless process or autocatalytic plating, involves the controlled application of metal coatings onto substrates through a chemical reduction process without the need for an external electrical power source. The hard Ni-B-based coatings are developed through the electroless process to achieve plain surfaces and enhance tribomechanical behaviour and corrosion resistance. The same method is also used to deposit Ni-B (ENB) coating, renowned for its tribological behaviour [1-3]. Electroless Ni-P coatings are well-regarded for their mechanical characteristics [4]. The deposition of elements like boron or phosphorus with nickel-based coatings increases the hardness of steel-made components [4,5]. The addition of boron and molybdenum with nickel during electroless plating imparts exceptional tribo-mechanical behaviour, making them highly desirable for various engineering applications.

The properties of chemically deposited coatings are usually changed due to alteration of composition [1,5,6]. It may further be changed through heat treatment [7]. The as-deposited ENB coatings usually possess an amorphous phase, which transforms into a crystalline phase after annealing [5,6,8]. This transformation is different for different coating compositions [7,8]. The ENB coatings usually exhibit a nanocrystalline phase if the amount of boron is less than 4 wt. %, which becomes amorphous upon an increase in boron more than 6.5 wt. % [8]. These modifications may result in changes in characteristics [6,9]. These changes in composition and phase structure lead to changes in tribo-mechanical behaviours of the coated layers applied over different substrate metals [9]. Similarly, the surface hardness usually follows the boron content in borohydride-reduced coatings [10], and it increases further upon annealing [10] due to the development of hard Ni_2B and Ni_3B phases [11-13].

The coated specimens developed with hard particles like W, Mo and ENB coating matrices have been deposited to study different properties [13-16]. The deposition of Ni-B-Mo coated layers is an important process in surface engineering. The Ni-B-Mo coatings showcase a uniform surface with cauliflower-like morphology [13]. The corrosion behaviour of Ni-B-Mo coated untreated specimens is enhanced upon phase transformation from amorphous to crystalline, and it is enhanced further due to annealing up to 550 °C [13]. The Ni-B-Mo coating exhibits thermal stability till up to 400 °C, as indicated by the unchanged surface hardness [13]. A comparative corrosion resistance of ENB-based binary and ternary coatings has been carried out in previous studies, which show that Ni-B-Mo coatings possess better corrosion behaviour than Ni-B and Ni-B-W [17]. On the other hand, the addition of hard nanosize ZrO_2, Al_2O_3 and TiO_2 may also change the coating characteristics. It is noticed that surface hardness and modulus of elasticity of ENB coatings are enhanced, possibly with grain refinement [16,18,19]. The electroless coatings are also deposited along with different nanoparticles like TiO_2 and Al_2O_3 to characterise based on various tribo-mechanical behaviours [20,21]. Electroless coatings are also being developed with or without the use of stabilizers [22,23].

Therefore, it becomes evident from the preceding literature studies that the behaviour of coatings is contingent upon factors like chemical composition, morphology, phase structure, etc. These characteristics, in turn, are influenced by heat treatment conditions. Additionally, chemical bath composition significantly impacts coating properties. The introduction of various elements with differing concentrations into the coating bath alters its composition, subsequently affecting the coating properties. However, the corrosion behaviour of autocatalytically developed Ni-B-Mo coatings has not been explored much, especially changes in corrosion resistance due to variations in coating bath composition and the impact of bath parameters. The previous study also explored only the variation in corrosion resistance of three different variants of coatings at three concentration levels [17]. However, the significance of individual parameter concentrations is not clear from that study [17]. Hence, there remains a need to analyse the impact of bath parameter concentrations on the corrosion resistance of untreated Ni-B-Mo coatings.

Hence, the current study is directed towards the development of Ni-B-Mo coatings with different bath parameter concentrations to analyse their importance on corrosion resistance. The bath elements, i.e. $NiCl_2$ and Na_2MoO_4 supply Ni and Mo ions, respectively. NaBH4 serves as the supplier of boron and the reducing agent. The investigations carried out in this study aimed to analyse and represent the impact of these parameters on corrosion resistance.

2. Coating development and investigation process

2.1 Coating development

Before starting the autocatalytic deposition process, the specimens are prepared using different methods. Finally, the substrates having smooth and defect-free surfaces are picked to deposit coatings over them. Initially, the substrates are cleaned with plain soap and water to remove dirt and then degreased with acetone. The substrates are further cleaned to obtain a rust-free or oil-free surface and then rinsed with deionized water. Now, the specimens are ready for final use, and they are further dunked into a half-heated $PdCl_2$ solution just before dipping the specimens into the chemical solution. AISI 1040 steel substrates are coated with Ni-B-Mo using the electroless technique, which may be seen in detail in the previous article [8].

Table 1. Coating bath compositions

Coating bath element	Function	Level 1	Level 2	Level 3	Level 4	Level 5
$NiCl_2$, g/l	source of Ni ion	10	15	20	25	30
$NaBH_4$, g/l	reducing agent; source of B ion	0.40	0.60	0.80	1.00	1.20
Na_2MoO_4, g/l	source of Mo ion	15	20	25	30	35
$C_2H_8N_2$, g/l	complexing agent	59				
NaOH, g/l	buffer	40				
$Pb(NO_3)_2$, g/l	stabilizer	0.0145				

The elements of the coating bath and the concentration ranges are displayed in Table 1. The coating is deposited with five different concentration levels and with varying concentrations of each parameter, as mentioned in Table 1. The concentrations of other parameters are maintained at Level 3 values, while each parameter is varied from Level 1 to Level 5. The chemical bath temperature is maintained at 85 °C and the pH is monitored intermittently to keep it at 12.5. The flat specimens' dimensions were 15 × 15 × 2 mm^3. Initially, the surface morphology and chemical composition were checked to ensure the effective application of coatings. A total of 4 hours was provided to deposit a thicker coated layer.

2.2 Characterisation

The coatings must be checked just after deposition to confirm the successful deposition. This was done through basic characterisation.

The coating thickness and morphology are analysed through a Hitachi S-3400N scanning electron microscope (SEM) at different magnifications. The set-up consists of a secondary electron detector, and the tests are conducted at 10 – 15 keV. The coatings are initially checked for thickness, which gives an idea of their successful deposition. The coated layer thickness is computed from the mass gain.

The coating composition also needs to be studied to ensure the further deposition of major elements, and it is done with Carl Zeiss Sigma energy-dispersive X-ray spectrometer (EDAX), which is operated at 10 keV.

The coating elements attach to the substrate surface and may remain present in different phases. The same phase structure is studied using Bruker D8 ADVANCE X-ray diffractometer (XRD) at a diffraction angle of 20 – 90°.

It is also necessary to study the surface texture of the coatings as it can also contribute to their corrosion behaviour. Hence, it is studied using a Taylor Hobson Surtronic 3+ profilometer. The set-up uses a diamond-made stylus that can move over the surface. The stylus tip has a radius of 5 µm, and the sampling length is 4 mm. The tests are conducted on three locations of the same specimen, and the average value of the arithmetical mean height *Ra* is presented.

The corrosion behaviour is investigated through a three-electrode-based ACM Instruments Gill AC potentiostat. The potentiostat uses two different methods. The details of the method employed in the current study are also elaborated on in a previous article [8]. The potentiostat used to perform the test employed an auxiliary electrode (AE), reference electrode (RE) and working electrode (WE), as mentioned in Figure 1. The AE facilitates the flow of applied current through the solution. The RE is used as a reference to measure the potential difference, and the WE, i.e. the specimen, is used as the working electrode. Only 1 cm^2 of WE is exposed to the 3.5 wt. % NaCl solution.

A settling time of 15 minutes was provided for the open circuit potential to be steady. The set-up is accompanied by a computer that records the data. The software Analysis (ACM Instruments) provided with the set-up is employed to study the corrosion results and obtain different plots from the recorded data of potentiodynamic polarization (PDP) and electrochemical impedance spectroscopy (EIS) tests.

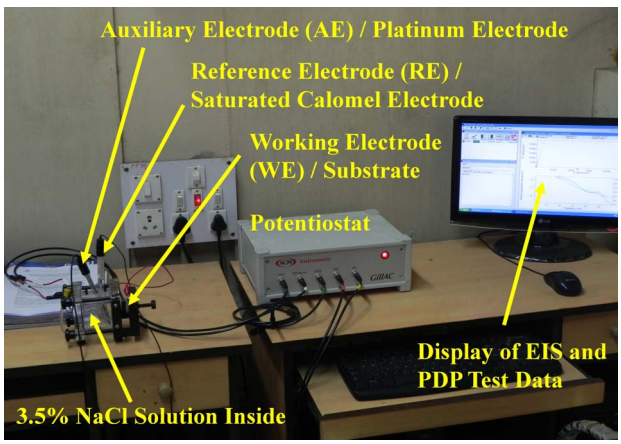

Figure 1. Corrosion test set-up

Figure 2 shows the equivalent circuit diagram for ideal and non-ideal behaviours used during the EIS test under the current study. The R_{sol} represents the resistance between the WE and RE. Figure 2b contains CPE_{dl}, which represents the double-layer capacitance for non-ideal behaviours [8]. The resistance experienced by the electrons during the transfer is termed as charge transfer resistance (R_{ct}). The same is also shown in Figure 2.

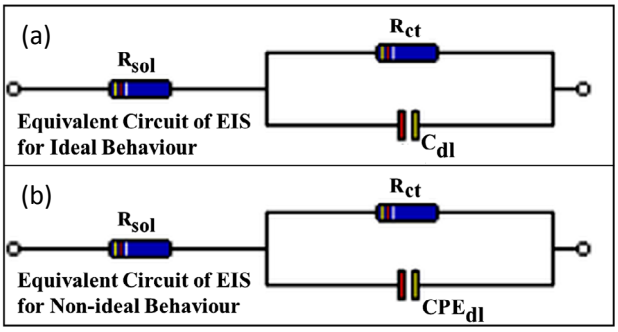

Figure 2. Equivalent circuit diagram for: (a) ideal behaviour and (b) non-ideal behaviour

The corrosion test mechanism is elaborated in Figure 3. The potentiostat in the corrosion test provides a positive voltage to the WE relative to RE. The anions potential is drawn towards the WE surface by the positive voltage. The solvent molecules around it come in touch with it once the anions get close to the electrode surface to form a capacitor. The electrochemical cell contains two oppositely charged electrodes set apart by a corrosive solution. This resembles a capacitor, which also contains two oppositely charged electrodes set apart by dielectric materials. Once the WE comes in touch with the corrosive medium, two layers of opposite charges form at the interface, which is called a double layer, as presented in Figure 3. Another electrode, termed an AE, remains present in the electrochemical cell. The AE is applied to polarise the RE. The AE can also be considered a source or sink of electrons for the reactions occurring at the working electrode surface.

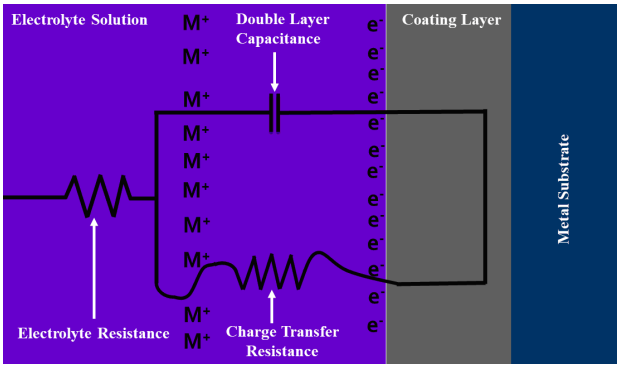

Figure 3. Corrosion test mechanism

The potentiostat contains a metal electrode on one side, which is the coated specimen, and a water-based electrode on the opposite side, which is the NaCl solution. Once a metal electrode comes in contact with the electrolyte, the ions in the electrolyte are absorbed into the working electrode surface. In Figure 3, the electrons or negatively charged ions are absorbed at the working electrode. Just after that, the ions with opposite charges come close to it to develop a double layer. Hence, it acts as a capacitor, and the corresponding capacitance is called double-layer capacitance (C_{dl}). At sufficient potential, the electrolyte can take electrons or release them, while the metal can come out from the working electrode and dissolve into the electrolyte or deposit over the working electrode. If any of these happens, this type of reaction is called an electrochemical reaction. This electrochemical reaction also gives rise to current, which can give rise to resistance, and it is called impedance.

3. Analysis of results and discussion

3.1 Coating thickness

The untreated coatings are first checked for successful application of layers. Earlier reports suggest that Ni-B coatings deposited in an autocatalytic process, containing approximately 5 wt. % boron generally exhibit a density of about 8.25 g/cm^3 [24]. Hence, considering the same density and uniformly coated layer, the mass gain is used to calculate the thickness. The same is also measured using SEM. Both results are in good agreement.

The coated layers observed under SEM are recorded in image form for each level of composition. However, only one is displayed in Figure 4a. The other layer thickness data are plotted against bath concentration level, which is shown in Figure 4b, showing an increasing trend with bath concentration level. The concentration of $NaBH_4$ increases with the bath concentration level. The objective of $NaBH_4$ is to take out metal ions. Therefore, the higher amount of $NaBH_4$ is expected to pull out extra metal ions, which means acceleration in the reduction reaction, and it leads to more metal ion extraction, resulting in an increase in coating thickness with bath concentration level.

Figure 4a also shows some columnar structure, which is very often seen in borohydride-reduced coatings [8,10,25,26]. The chemical salts in the

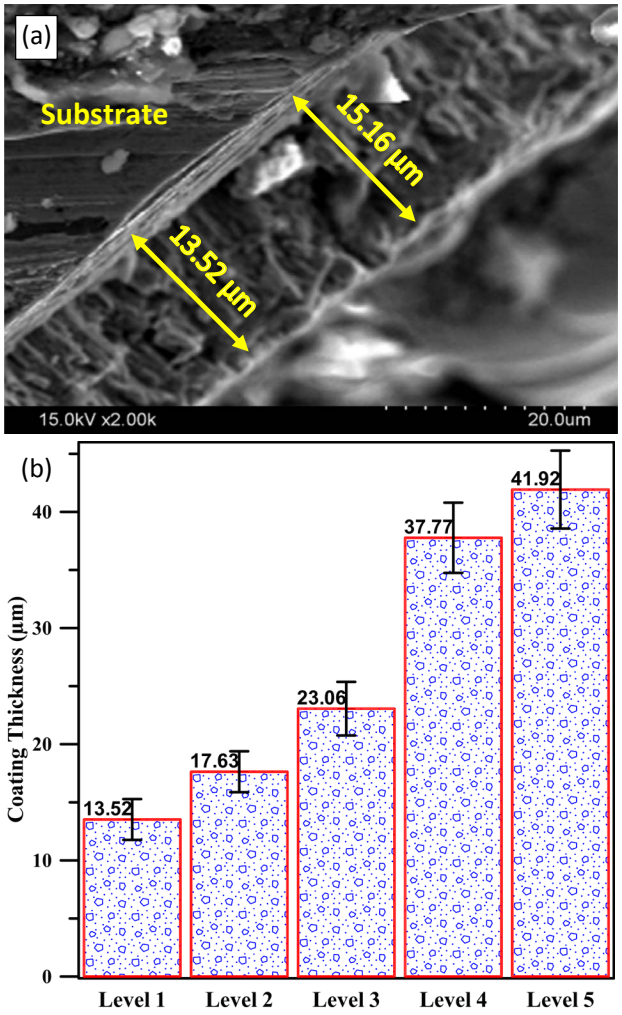

Figure 4. Coating thickness: (a) SEM image of coating thickness and (b) comparative coating thickness plot

chemical solution start reacting at a specific temperature around 70 °C, which is higher than room temperature [27,28]. The reduction reaction accelerates because of the temperature rise. The metal ions start depositing at the substrate surface at different nuclei points, and they grow gradually with time in a vertical direction. The deposition of metal ions in the vertical direction makes it a columnar structure. The uniform distribution of the columnar structure ultimately forms a cauliflower-like morphology.

3.2 Surface morphology

The successful application of coatings is confirmed by mass gain and thickness observation. The surface morphology observation results are recorded as SEM images and displayed in Figure 5. Overall, coated surfaces appear to be bright at lower concentrations, but they contain some cracked morphology, as detected with SEM and demonstrated in Figure 5a. The same coated surfaces become grey-coloured and darker with increased bath concentration levels [5,11]. Moreover, the Ni-B-Mo coatings contain a cauliflower-like morphology formed due to the uniform distribution of nodules. The earlier reports [1,2,26,29] also suggest the same trend. The nodular morphology is known to favour the improvement in tribological behaviour. Hence, it is widely applied for tribological applications as it reduces the real contact area and decreases the coefficient of friction [1,29]. As mentioned earlier, the extracted metal ion deposition begins at various nucleation sites of the substrate surface and restricts the growth in the side direction. Hence, it is forced to deposit the ions along a vertical direction, forming a columnar structure and ultimately resulting in a cauliflower-like morphology [8,27].

The addition of Mo into the Ni-B coating resulted in the development of high stress. Different thermal expansion coefficients of the substrate and coated layer may also develop stress, resulting in cracked morphology. While the concentration level increased, more metal ions were extracted, and a thicker coated layer was deposited. The higher amount of metal ions might have made a closely packed coated surface with a uniform distribution of nodules. The thicker coated layer might be able to resist the high stress and form a compact, uniform surface. However, the compact surface also possesses some surface boundaries. The coated surfaces contain comparatively more compact surfaces compared to Level 1. However, the surfaces developed at Level 4 and Level 5 possess wide surface boundaries. The surface crack and surface boundaries are very much prone to corrosion attack.

3.3 Coating composition

The presence of major elements like Ni, B and Mo are checked and confirmed through EDAX. The EDAX results obtained for five different bath concentration levels are shown in Figure 6. The existence of these elements is supported by the presence of the sharp peaks in all EDAX spectrums corresponding to Ni, B and Mo. The EDAX also detects and records the amount of these elements in the coatings, which is given in tabular form for each level. It depicts that the coating at Level 1 contains 91.70 wt. % nickel, 3.70 wt. % boron and 3.10 wt. % molybdenum. The amount of these elements in the coating varies with bath concentration level. The presence of both boron and molybdenum is found to increase with bath concentration level.

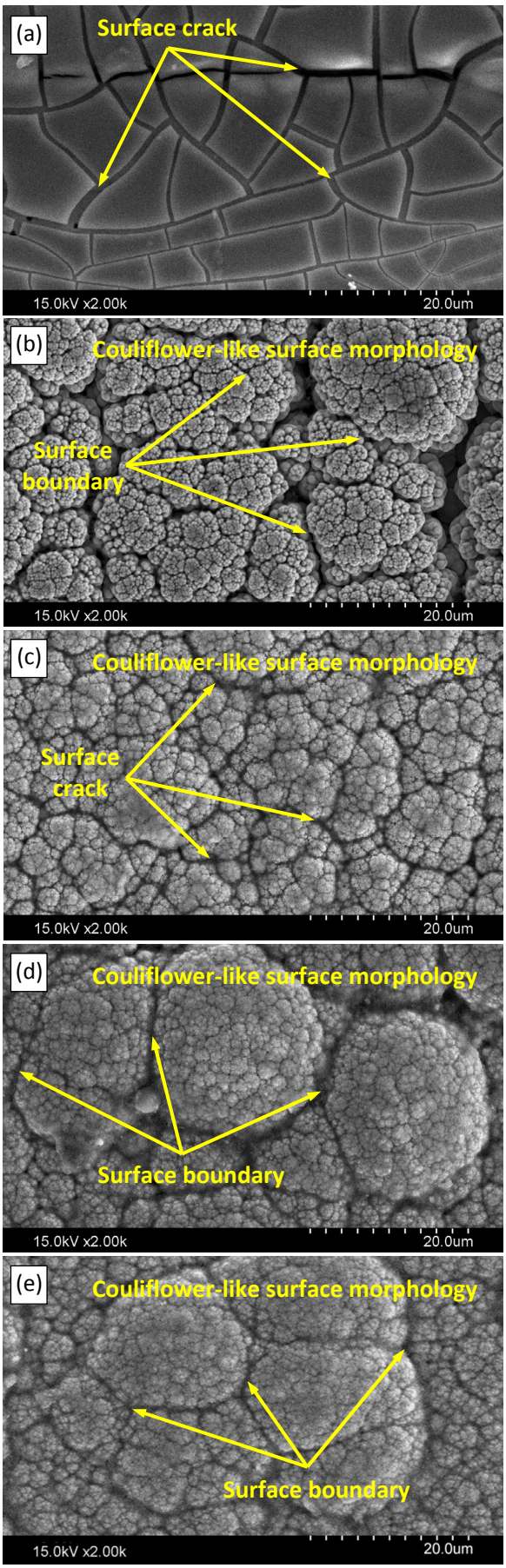

Figure 5. SEM images of Ni-B-Mo coatings obtained at coating bath concentration of: (a) Level 1, (b) Level 2, (c) Level 3, (d) Level 4 and (e) Level 5

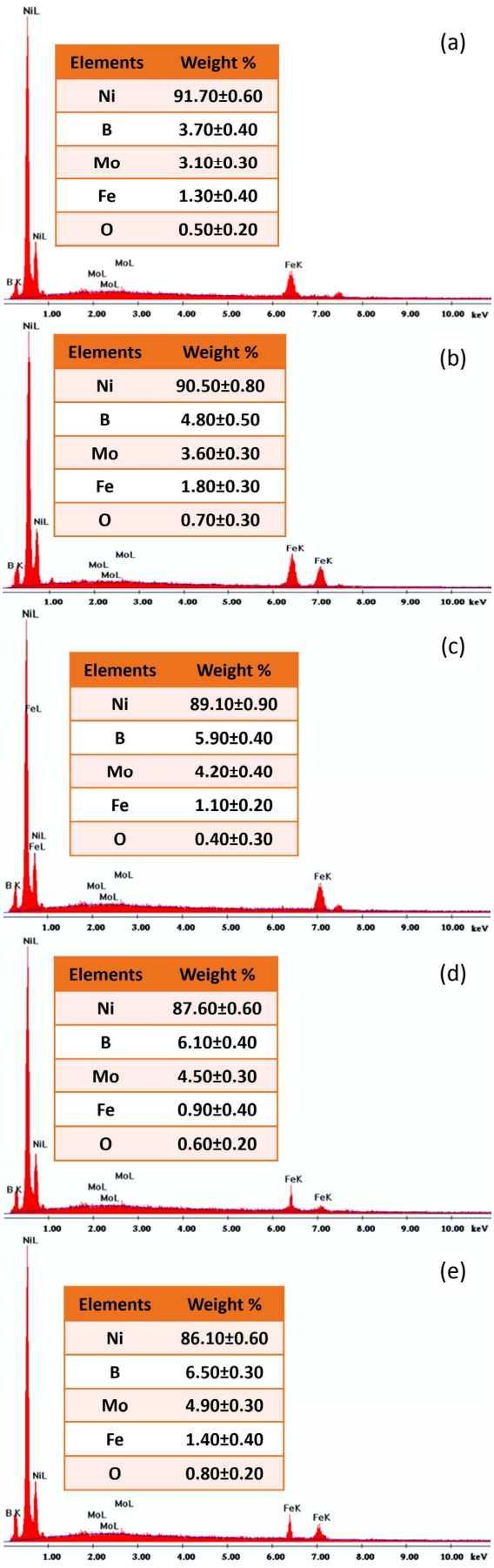

Figure 6. EDAX result of the Ni-B-Mo coatings obtained at coating bath concentration of: (a) Level 1, (b) Level 2, (c) Level 3, (d) Level 4 and (e) Level 5

As discussed earlier, a change in $NaBH_4$ concentration may impact the formation of coatings with a change in its basic features, which may ultimately change coating behaviours. The boron content in the coatings improved with $NaBH_4$ [6,26]. The sodium molybdate and sodium borohydride concentrations are increased with increased concentration levels, which means Mo and B ions are also improved. Hence, this rise in the respective ions ultimately leads to an increase in their presence. The rise in $NaBH_4$ content also accelerates the reduction reaction process and extraction of a higher amount of metal ions. This higher amount of metal ions may be correlated with the improvement in boron and molybdenum content in the coatings.

Conversely, the increase in boron and molybdenum contributes to a diminution in nickel content in the coatings [8,26]. The nickel content has decreased from 91.70 to 86.10 wt. %. On the other hand, the boron content is increased from 3.70 to 6.50 wt. % and the molybdenum also increased from 3.10 to 4.90 wt. % with the increased concentration from Level 1 to Level 5. However, the presence of molybdenum is lower than that of boron, which is aligned with previous studies [26]. The EDAX results also contain certain peaks of Fe and O, which confirm their presence in the coatings but not a very insignificant amount and hence may be neglected.

3.4 Phase structure

The coated layer adheres to the substrate surface and exits in different phases. The presence of these phases is identified through XRD and the obtained XRD patterns are presented in Figure 7. The XRD patterns may contain hump or sharp peaks in it. The hump is an indication of the amorphous phase and the sharp peak corresponds to the crystalline phase. If the hump and sharp peaks both exist together in an XRD pattern, then it indicates the coexistence of both phases.

The XRD spectrum of as-deposited Ni-B-Mo coated specimens until Level 2 contains only a hump and a sharp peak at 45°, and it affirms the coexistence of an amorphous-crystalline phase [6,25]. The sharp peak at 45° corresponds to the crystalline phase of Ni (111) [13]. The XRD spectrum of the same coating also contains two more sharp peaks at 65 and 83° [9,30]. Those sharp peaks are nothing but the crystalline peaks of Fe.

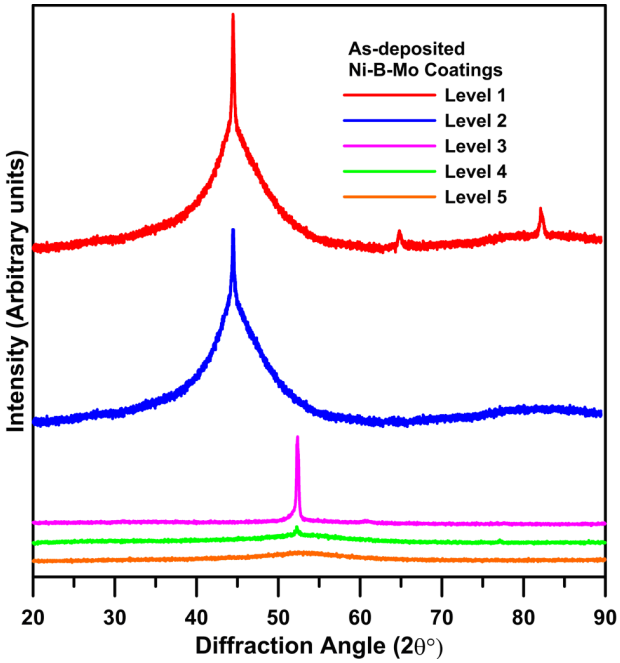

Figure 7. XRD pattern of as-deposited Ni-B-Mo coatings

The hump flattened slightly at Level 3, and it also possesses a similar peak at 53°. The flattening of the XRD pattern indicates the conversion of phase towards the amorphous phase. The sharp peak at 53° also represents the crystalline phase of Ni (200) [13]. The untreated Ni-B-Mo coated specimens developed up to Level 3 possess the amorphous and crystalline phases together [13], though the crystallinity decreased as the bath concentration level increased. It has been reported previously that ENB coatings display a similar trend [13].

Generally, the ENB coatings with 4 wt. % boron content or lower contain crystalline and amorphous phases [6,31]. It is also reported that the rise in boron in ENB coatings promotes amorphous phase formation [32]. The sharp crystalline peak diminished with bath concentration level [6,27]. The boron content is also improved with bath concentration level. The ENB-coated specimens having boron content higher than 6.5 wt. % generally encourages the development of the amorphous phase by restricting the nuclei formation [32]. The untreated Ni-B-Mo coated specimens are noticed to contain 3.70 wt. % boron at Level 1, which gradually increased to 6.50 wt. % at Level 5. Similarly, molybdenum content also increased from 3.10 to 4.90 wt. % with the increased bath concentration level. It is also reported that the addition of molybdenum into the coating promotes amorphous phase development as it restricts nuclei formation [33]. Hence, the increased

concentration of molybdenum and boron favours amorphous phase formation. On the other hand, a lower amount of boron and molybdenum is the reason for the existence of the amorphous-crystalline phase.

The peak corresponding to Fe is detected in both the EDAX and XRD results. Characterisation methods like EDAX and XRD are direct and straightforward [30]. The results obtained from these methods may vary depending on different elements like coating thickness, surface roughness, etc. [30]. The coated layer thickness at Level 1 is minimal, and it also contains cracked morphology. Hence, the lower coating thickness with cracked surface morphology conforms to the presence of Fe in EDAX and XRD patterns.

3.5 Surface roughness

Once the coatings are characterised based on their basic features, the coated surfaces are checked for surface roughness, as it may play a vital role in deciding their corrosion behaviour. The variation in arithmetical mean height (*Ra*) value is observed and recorded against bath concentration level and each varying bath parameter. The results of those observations are presented in Figure 8. The *Ra* value of uncoated specimens is 0.285 µm.

It is seen that the coated surface becomes smoother compared to the uncoated one when the coatings are produced with Level 1 of bath composition, as may be seen in Figure 8a. The surface roughness continues to increase with a

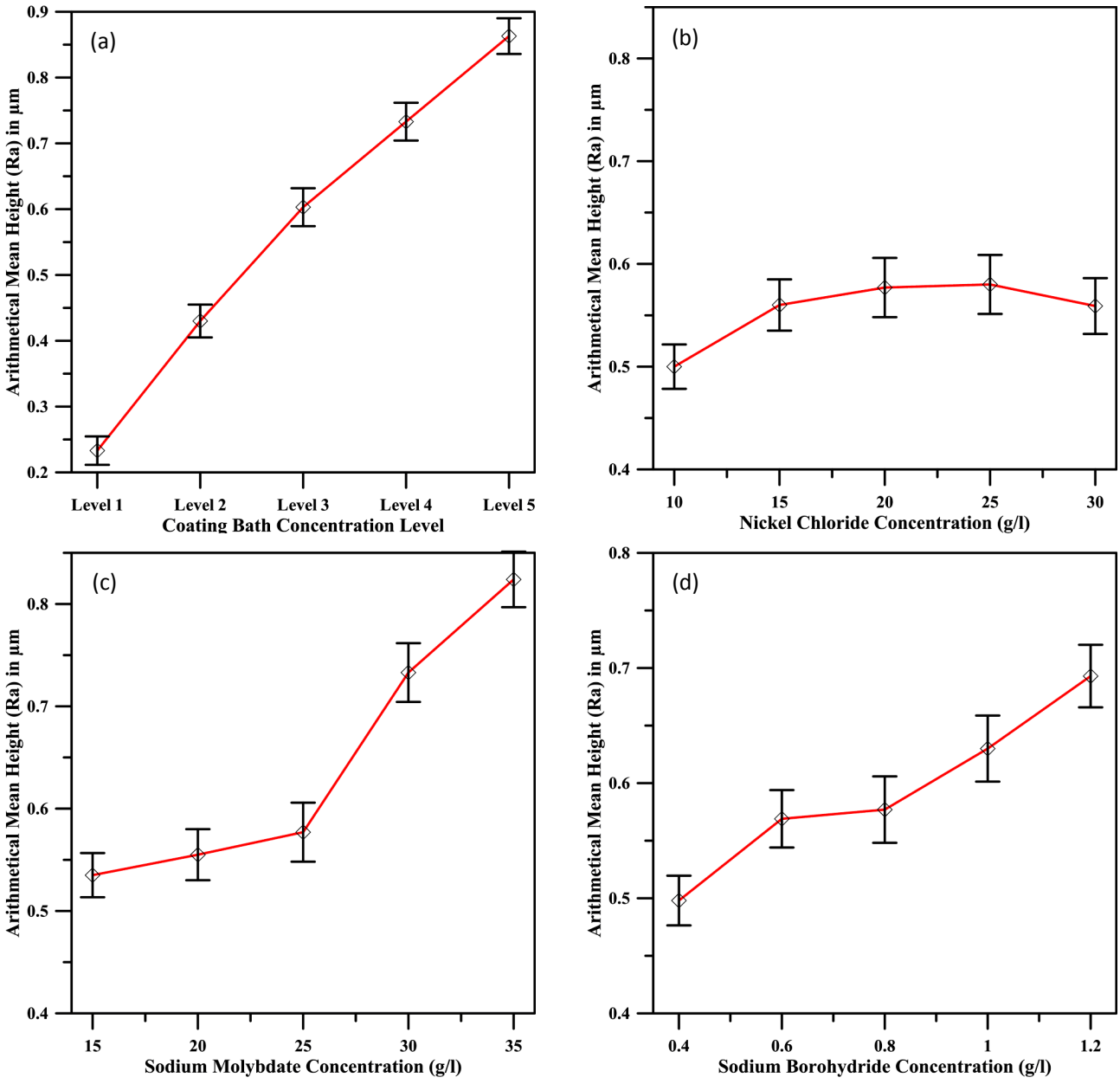

Figure 8. Surface roughness variation with the concentration of: (a) coating bath, (b) $NiCl_2$, (c) $NaBH_4$ and (d) Na_2MoO_4

further increase in bath concentration level. The trend of surface roughness with $NiCl_2$ variation is demonstrated in Figure 8b. The *Ra* value slightly increased with $NiCl_2$ concentration of 25 g/l and then decreased. However, this change is not very big, especially within the 15 – 25 g/l range. Nevertheless, the surface roughness remained higher than the uncoated specimen within its working range. The $NiCl_2$ concentration ranges from 10 – 30 g/l. Hence, the increase in $NiCl_2$ concentration might have dominated the coating deposition and partially redistricted the rougher surface formation.

The $NaBH_4$ plays a vital role in extracting metal ions and coating deposition. The surface roughness trend with $NaBH_4$ concentration is presented in Figure 8c, and it is an increasing trend. The ion reduction process accelerates due to an increment in $NaBH_4$ concentration [1,2,34,35], leading to random deposition of ions, resulting in a rougher surface formation. Including molybdenum in ENB coating is seen to develop cracked morphology, resulting in a rougher surface formation. The surface roughness variation with Na_2MoO_4 concentration is presented in Figure 8d, which clearly depicts an increase in *Ra* value with Na_2MoO_4 concentration throughout its working range. Both $NaBH_4$ and Na_2MoO_4 contributed to the increase in surface roughness, which can be correlated with the increase in roughness value with the increased bath concentration level.

Overall, the surface roughness increased with the bath concentration level primarily because of the increased $NaBH_4$ and Na_2MoO_4 concentrations. Firstly, $NaBH_4$ is a reducing agent and source of boron ions. The main objective of $NaBH_4$ is to extract metal ions in the chemical solution. Hence, the ion reduction rate should increase with its concentration increase and deposit them over the steel substrate randomly, resulting in a rougher surface development [1,2,34,35]. Secondly, Na_2MoO_4 is included in the coating solution to supply molybdenum ions, resulting in rougher surface formation with some visible cracks [13,26]. The rougher surface development may be correlated with the development of high stress because of the inclusion of Mo in ENB coating [13, 26]. Thirdly, it is seen that the metal salts do not interact under room temperature. Hence, it becomes necessary to increase the coating bath temperature since the reduction process is seen to initiate at around 70 °C [27,28]. The same chemical reaction gets faster with increased coating bath temperature and stables at around 85 – 90 °C [35,36]. The ion reduction process reaches its peak at the same temperature. Therefore, a higher number of ions are expected at this temperature, and they are supposed to attach to the substrate randomly. This type of random and faster ions deposition results in a rougher surface. The temperature effect is not considered, as the temperature is kept constant. Therefore, the increased reduction rate and high-stress growth due to molybdenum addition are perhaps linked to the increased surface roughness. The establishment of the rougher surface with cracked surface morphology because of high-stress growth is displayed in Figure 5a. Therefore, the surface roughness result is in good agreement with the characterisation results.

3.6 Corrosion resistance

The corrosion test results obtained from EIS and PDP methods are presented with the help of the Tafel and Nyquist plots, as shown in Figures 9 to 12. The data obtained from those plots are presented in tabular form in Table 2. The Nyquist plots typically contain a semi-circular loop. It becomes bigger with the increase in corrosion resistance and vice-versa [5]. The Tafel plot is obtained considering the corrosion potential (E_{corr}) along the *y*-axis and the log value of corrosion current density (I_{corr}) along the *x*-axis. The higher value of E_{corr} and the lower value of I_{corr} indicate an enhancement in corrosion resistance [37,38]. The R_{ct} and C_{dl} value is determined from the EIS test. The higher value of R_{ct} indicates better corrosion resistance.

Figure 9 demonstrates the corrosion behaviour of untreated coated specimens with bath concentration level change. Figure 9 shows that the corrosion resistance increases with the bath concentration level up to Level 3. It deteriorates upon further increase down to Level 5. The corrosion behaviour of coated specimens usually deviates due to different factors like coating composition, surface morphology, texture, surface crack, surface roughness, etc. [16]. The change in composition, like an increment in boron into ENB coatings, enhances performance against corrosion [5,13,30]. The rougher surface texture or rough surface, surface morphology with wide surface boundary and surface cracks are the favourable sites for corrosive medium to enter through it, resulting in deterioration in corrosion resistance [13,30].

Table 2. Corrosion test results

Parameter	EIS test		PDP test		Corrosion rate × 10^{-4}, mm/year
	$R_{ct} \times 10^4$, Ω cm^2	$C_{dl} \times 10^{-5}$, F/cm^2	$I_{corr} \times 10^{-4}$, mA/cm^2	E_{corr}, mV	
Variation in corrosion resistance with coating bath concentration level					
Level 1	0.735	7.135	53.247	−492.35	3.863
Level 2	1.041	0.165	25.219	−469.15	2.696
Level 3	3.323	7.384	9.386	−418.87	0.855
Level 4	1.739	5.954	19.579	−465.28	1.614
Level 5	0.751	6.486	49.532	−492.35	3.783
Variation in corrosion resistance with nickel chloride concentration					
10 g/l	1.271	4.014	54.240	−490.41	2.208
15 g/l	1.266	8.470	51.115	−485.79	2.217
20 g/l	3.323	7.384	9.386	−418.87	0.085
25 g/l	2.675	13.310	18.866	−450.43	1.049
30 g/l	2.354	2.548	17.957	−464.05	1.185
Variation in corrosion resistance with sodium borohydride concentration					
0.40 g/l	1.156	13.230	36.607	−462.02	2.428
0.60 g/l	1.714	6.062	11.062	−454.43	1.638
0.80 g/l	3.323	7.384	9.386	−418.87	0.085
1.00 g/l	0.677	6.096	73.832	−478.26	4.144
1.20 g/l	1.090	3.394	42.841	−478.21	2.575
Variation in corrosion resistance with sodium molybdate concentration					
15 g/l	1.983	31.430	14.685	−451.12	1.416
20 g/l	2.288	1.618	12.841	−454.43	1.066
25 g/l	3.323	7.384	9.386	−418.87	0.085
30 g/l	1.633	16.250	19.963	−472.93	1.638
35 g/l	1.086	3.510	35.502	−478.21	2.585

The coatings obtained with Level 1 bath concentration and the morphology presented in Figure 5a show some visible cracks. The visible crack is expected to permit the corrosive NaCl solution to enter, lowering the coating's capability to withstand corrosion. Figure 9a represents the plot having two semi-circular loops at Level 1 bath concentration, indicating that the NaCl solution might have passed through the surface crack and reached the substrate. The first loop depicts the corrosion performance of the coated layers, and the other loop is for the substrate material. However, the surface becomes compact due to further growth for bath concentration up to Level 3, as presented in Figures 5b and 5c. The coated surfaces developed with bath concentration above Level 3 are comparatively compact but possess some wider surface boundaries, as may be seen in Figures 5d and 5e. The wider surface boundaries may have been exposed to NaCl solution, which may have entered across the gaps. The penetration of NaCl solution confirms a deterioration of corrosion behaviours. However, the NaCl solution failed to reach the substrate surface, which can be confirmed by the presence of a single semi-circular loop in the Nyquist plot.

The obtained EIS (R_{ct} and C_{dl}) and PDP (E_{corr} and I_{corr}) test results are presented in Table 2, which represents an increase in R_{ct} value with bath concentration up to Level 3, and it decreased upon further rise in level. The E_{corr} value increased, i.e. E_{corr} value changed from −492.35 to −418.87 mV. On the other hand, the I_{corr} value decreased from 53.247 to 9.386 mA/cm^2. Both parameters indicate an improvement in corrosion resistance. A higher value of R_{ct} and a lower value of C_{dl} demonstrate an enhancement in corrosion behaviour [8,13,16]. An increase in the E_{corr} value and a decrease in the

I_{corr} value is also a sign of improvement in corrosion behaviour [8,13,16]. Hence, both the EIS and PDP tests show similar results. Table 2 and Figure 9 are well aligned with each other.

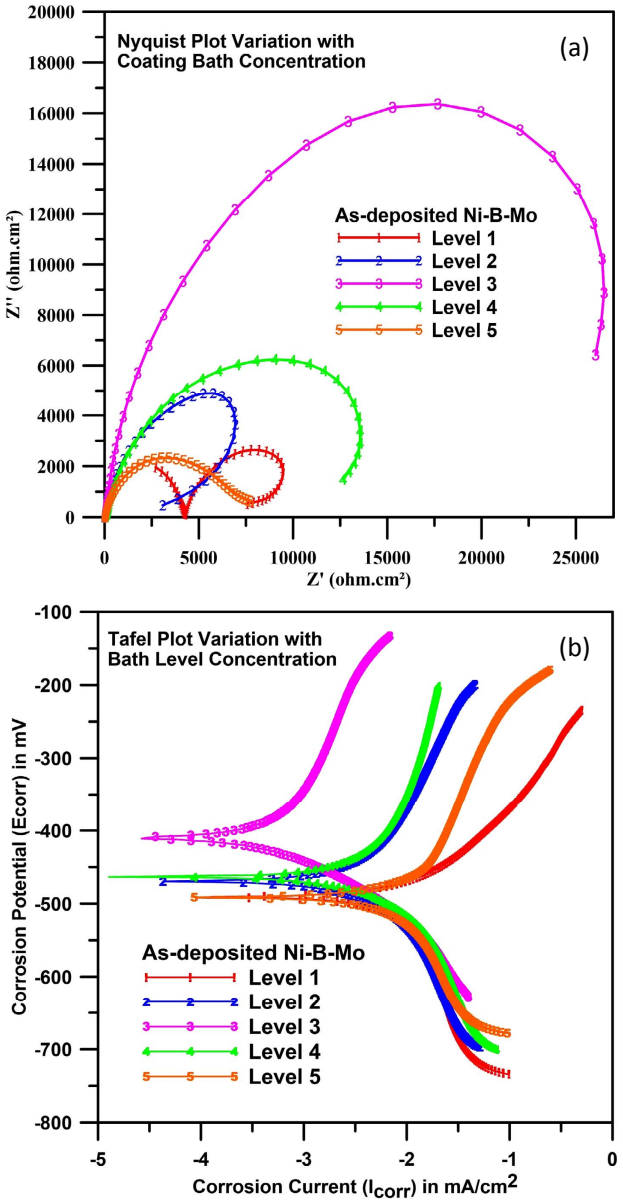

Figure 9. Corrosion resistance variation with coating bath concentration level: (a) Nyquist plot and (b) Tafel plot

The presence of boron in ENB-coated specimens is seen to improve with $NaBH_4$ [5], and the $NaBH_4$ content in the solution increased with bath concentration level, which led to an improvement in boron from 3.70 to 6.50 wt. %. The corrosion behaviour of ENB-coated specimens is determined by the presence of boron [5,6]. Therefore, a higher amount of boron is expected to enhance the ability to withstand corrosion. However, the inclusion of Mo in ENB coating results in a rougher surface caused by the development of high stress, which ultimately reduces the corrosion resistance at higher concentrations [8,13]. Initially, the ability of Ni-B-Mo coated layers to withstand corrosion increased, possibly because of boron content. The same is seen to deteriorate upon further increase in Na_2MoO_4 content.

The fluctuation in corrosion behaviour due to variation in $NiCl_2$ content is presented in Figure 10. It demonstrates an improvement in the corrosion behaviour of untreated Ni-B-Mo coated specimens because of an increase in $NiCl_2$ from 10 to 20 g/l. The corrosion behaviour deteriorates upon further increase in $NiCl_2$ concentration up to 30 g/l. However, the ability to withstand corrosion for the coated specimens developed at 25 and 30 g/l remained higher than the coating obtained with 10 g/l of $NiCl_2$. Generally, corrosion resistance deteriorates with increased *Ra* value. The *Ra* also increased with $NiCl_2$ concentration, which is just the opposite of the usual trend. The incorporation of an increased $NiCl_2$ concentration might have filled the gaps between the grain boundaries, resulting in an enhancement in corrosion resistance.

However, the coated surfaces become smoother with increased nickel chloride concentration from 25 to 30 g/l, probably due to the smoothening of the surface upon the inclusion of Ni ions. Conversely, increased $NiCl_2$ concentration might have increased the Ni ions and restricted the boron ion deposition. The reduction in boron content usually results in a reduction in the corrosion behaviour of boron-based coated specimens. Hence, the deterioration of corrosion behaviour with increased $NiCl_2$ concentration is possibly due to a reduction in the presence of boron. Overall, the untreated Ni-B-Mo coated specimen developed at 20 g/l had the best corrosion resistance, while the specimen developed at 10 g/l had the worst.

The corrosion behaviour of untreated Ni-B-Mo coated specimens developed by varying $NaBH_4$ from 0.40 to 1.2 g/l is shown in Figure 11. It demonstrates an improvement in corrosion resistance with NaBH4 concentration from 0.40 to 0.80 g/l. With further increase in $NaBH_4$ concentration, corrosion resistance decreases below the corrosion resistance of 0.40 g/l specimen. It is well known that the boron content is followed by the corrosion resistance of ENB-based coatings [5]. The presence of boron in ENB-based coated specimens increases due to the increase of borohydride concentration in the coating bath [6,11]. The characterisation results also show a

rising trend of boron due to increased $NaBH_4$ concentration. However, the presence of $NaBH_4$ increases the surface roughness, which may be seen in Figure 8c, and it is supposed to worsen the corrosion behaviour. The formation of the rougher surface with increased $NaBH_4$ concentration may be linked with the acceleration of the chemical reaction process and random deposition of ions [6,26]. The ability to withstand the corrosion of boron-based coated surfaces usually increases due to an increase in $NaBH_4$ concentration [6,11]. Therefore, this improvement in corrosion behaviour up to 0.80 g/l of $NaBH_4$ can be correlated with increased boron content and the deterioration of corrosion resistance after 0.80 g/l of $NaBH_4$ may be correlated with the rougher surface formation.

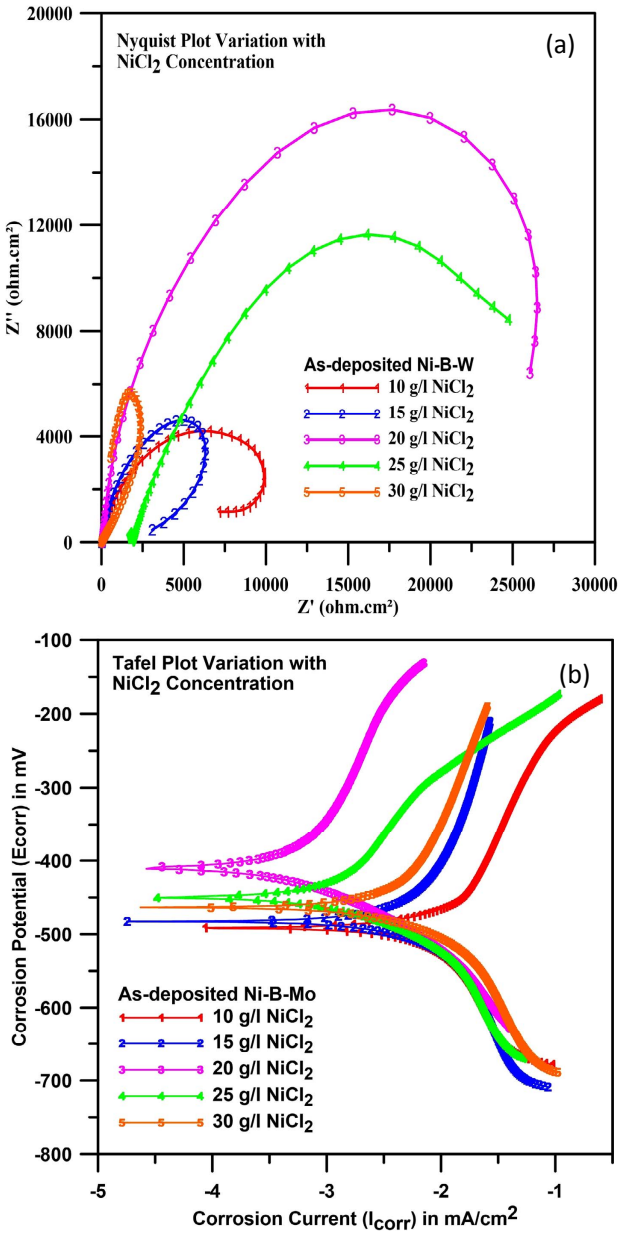

Figure 10. Corrosion resistance variation with $NiCl_2$ concentration: (a) Nyquist plot and (b) Tafel plot

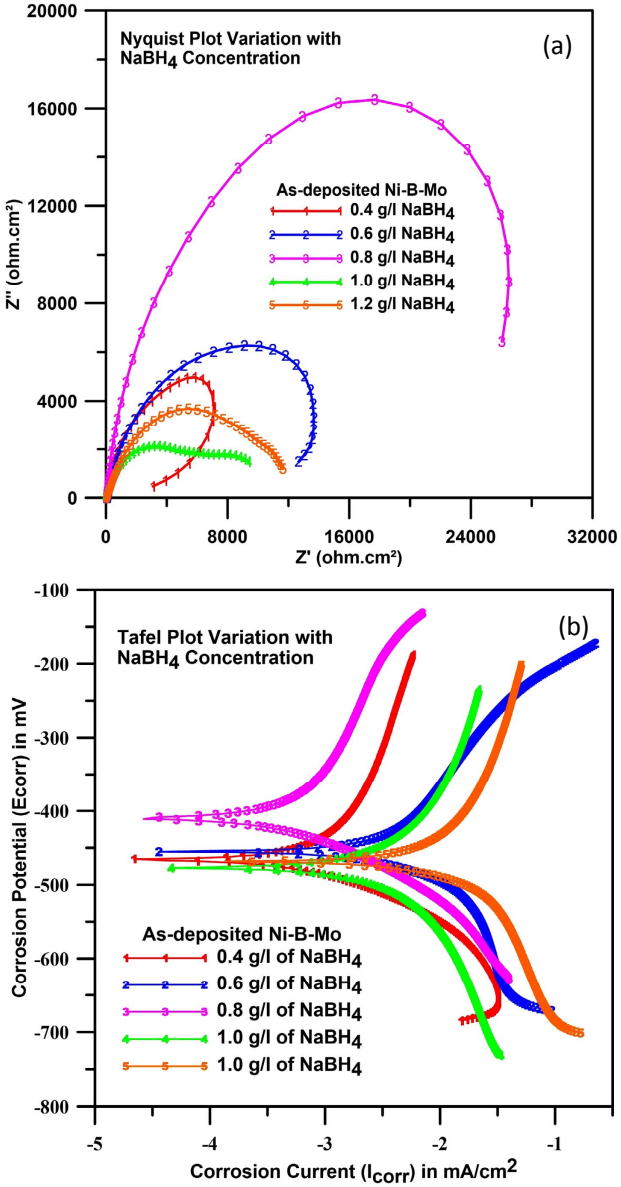

Figure 11. Corrosion resistance variation with $NaBH_4$ concentration: (a) Nyquist plot and (b) Tafel plot

The presence of boron and molybdenum in coatings increased due to $NaBH_4$ and Na_2MoO_4 concentration, respectively, which is evident from the EDAX results as displayed in Figure 6. It is also noticed in Figure 8 that the surface roughness also increases because of an increase in $NaBH_4$ and Na_2MoO_4 concentration. The variation in corrosion resistance with Na_2MoO_4 concentration is shown in Figure 12, which demonstrates an enhancement in corrosion resistance up to Na_2MoO_4 concentration of 25 g/l. The corrosion resistance is seen to reduce with further increase of Na_2MoO_4 concentration up to 35 g/l. An increase in boron content in ENB-based coatings usually improves coatings' ability to resist corrosion attack [31]. On the other hand, *Ra* value is also seen to increase

with $NaBH_4$ and Na_2MoO_4 concentration. The increased $NaBH_4$ concentration speeds up the ion extraction process, resulting in a random deposition of ions and a rougher surface formation. The wider surface boundary or rough surface texture usually favours the NaCl solution to enter through the surface boundaries, which is supposed to reduce corrosion resistance. It is seen in Figure 5a that the untreated Ni-B-Mo coated specimens developed at Level 1 concentration possess cracked morphology, which can act as an active corrosion site. The same untreated Ni-B-Mo coated surface turns into a rougher morphology due to the incorporation of Mo in ENB coating, ultimately decreasing its ability to withstand corrosion [38].

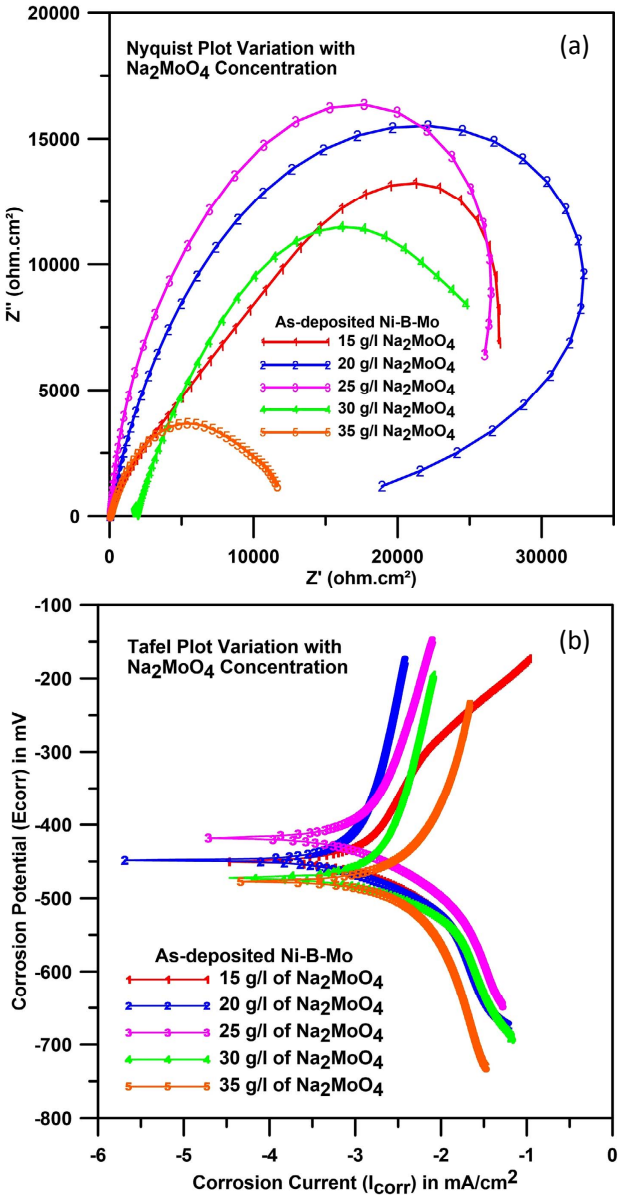

Figure 12. Corrosion resistance variation with Na_2MoO_4 concentration: (a) Nyquist plot and (b) Tafel plot

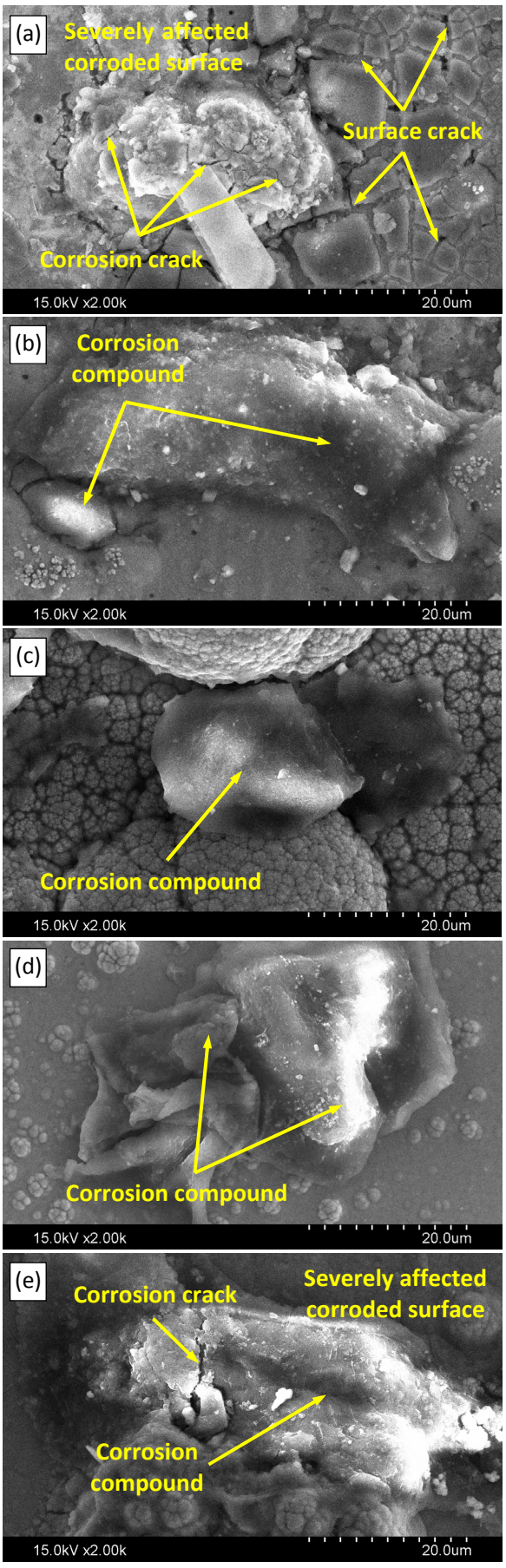

Figure 13. Corroded surface morphology obtained at coating bath concentration of: (a) Level 1, (b) Level 2, (c) Level 3, (d) Level 4 and (e) Level 5

The presence of boron generally improves the ability of coatings to resist corrosion attack by restricting the entry of NaCl solution through surface cracks or grain boundaries. Therefore, the increased corrosion resistance up to Level 3 could be linked to the higher amount of boron. The untreated Ni-B-Mo coated specimens obtained at concentration Level 3 possess closely packed and uniform distribution of nodules, which is suitable for resisting corrosion attack. A comparable pattern of increased corrosion resistance has been documented in earlier research [19,39]. The untreated Ni-B-Mo coated specimens developed at higher concentration levels possess some cluster of nodules, which creates wider surface boundaries. The rise in molybdenum and rougher surface morphology with open surface boundaries may have deteriorated the ability to withstand corrosion attack. The coating developed at Level 1 concentration possesses cracked morphology, resulting in a reduction in corrosion performance.

The untreated Ni-B-Mo coated specimens undergone corrosion tests are also examined under SEM. The SEM results are recorded in image form, which is presented in Figure 13. It depicts that the tested surfaces contain corrosion by-products placed on top of an uncoated substrate. The presence of those corrosion by-products is a sign of corrosion attack.

All the coated surfaces contain some corrosion by-products over the corroded surface. However, coatings that developed a small amount of corrosion by-products with some spongy appearance are the least affected ones. The same surface may also be seen in Figure 13c. The untreated specimens developed at Level 5 underwent a corrosion attack and are observed to contain corrosion by-products with some corrosion cracks, as presented in Figure 13e. Hence, the Ni-B-Mo coating's capability to prevent corrosion attack at Level 5 is the lowest compared to other variants. The resistance against corrosion of borohydride-reduced coatings varies with phase structure and

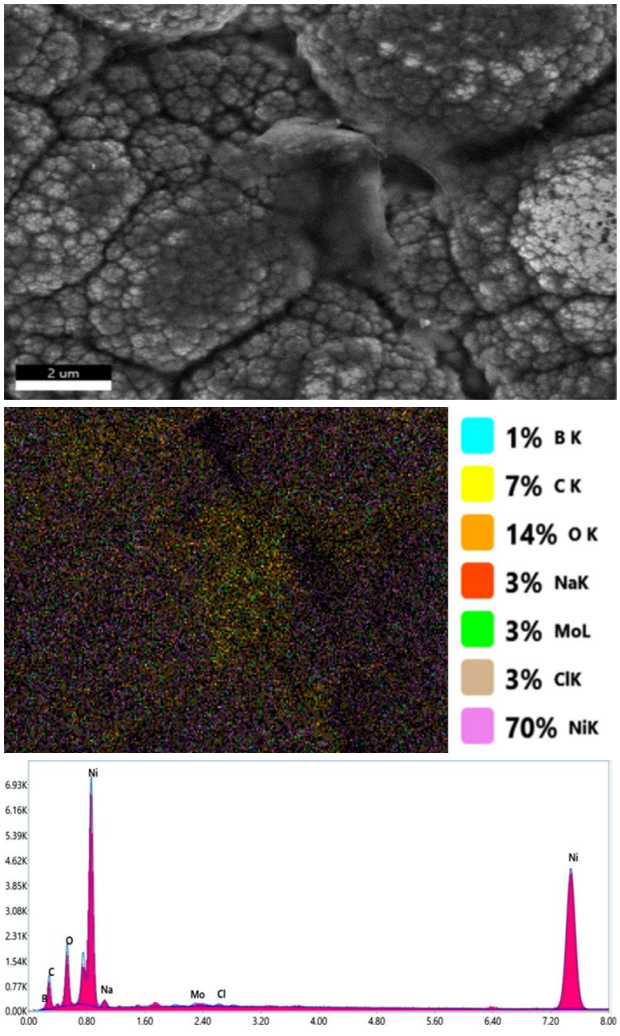

Figure 14. EDAX result of corroded surface obtained at bath concentration Level 1

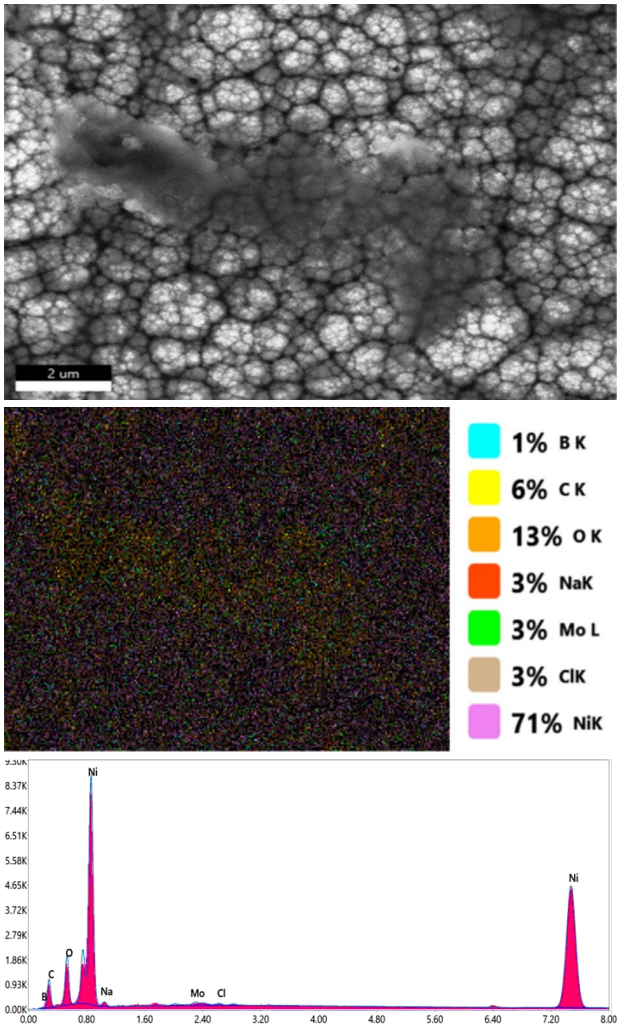

Figure 15. EDAX result of corroded surface obtained at bath concentration Level 2

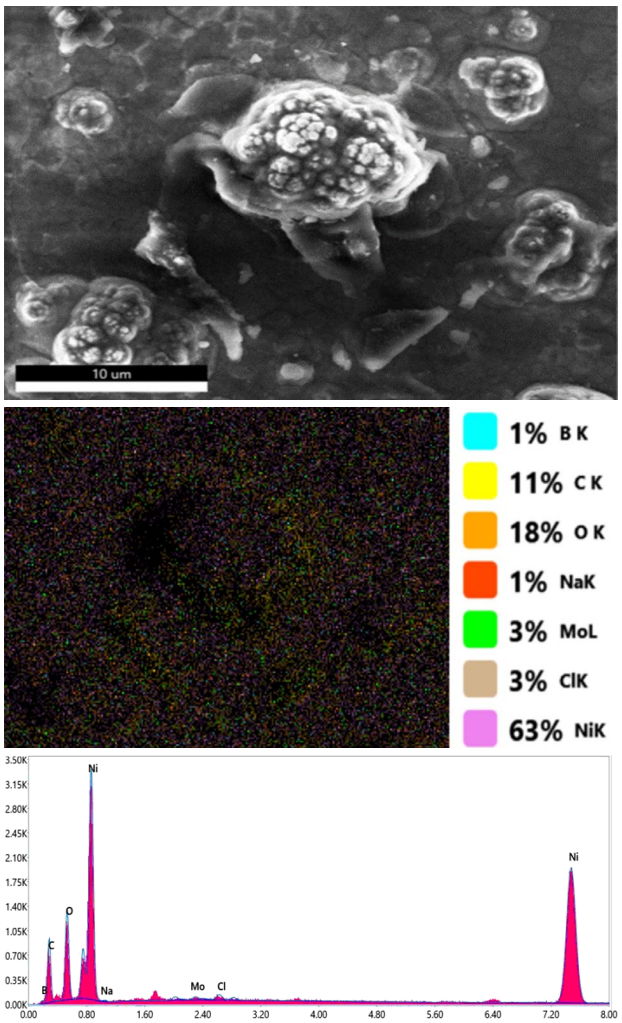

Figure 16. EDAX result of corroded surface obtained at bath concentration Level 3

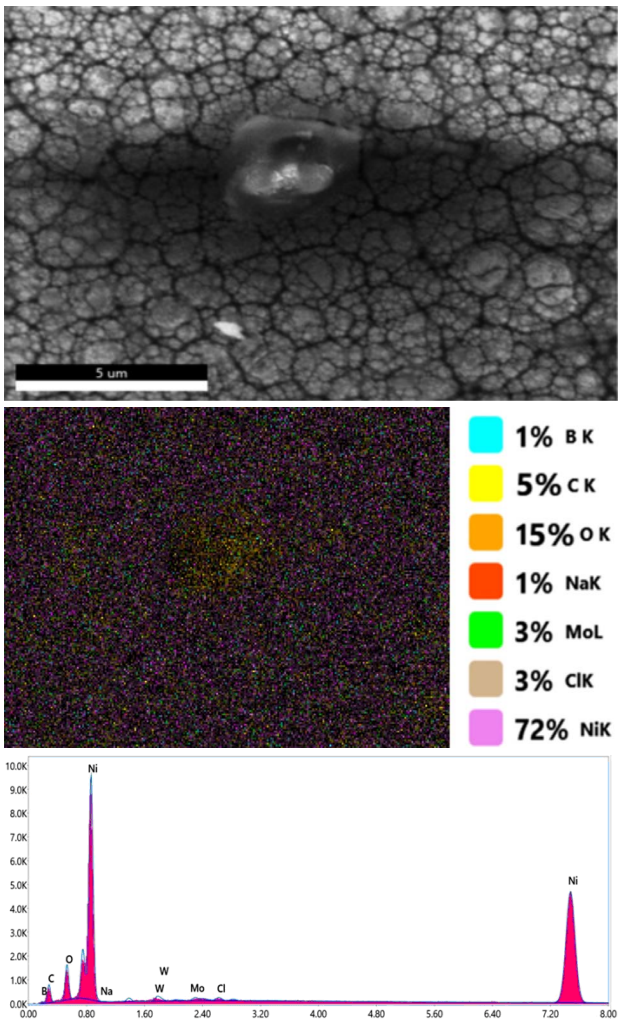

Figure 17. EDAX result of corroded surface obtained at bath concentration Level 4

surface morphology [40]. It was reported earlier that coatings with amorphous phases generally show better resistance against corrosion attacks compared to coatings with nanocrystalline phases [1,40]. The amorphous nanocrystalline phase of boron-based coatings with low boron is transformed into an amorphous phase upon increased boron content. This phase transformation into amorphous may also contribute to the ability to withstand corrosion enhancement. Hence, the phase structure of the coatings, shown in Figure 7, shows the changes in phase and is well aligned with the corrosion test results and the corroded surface SEM results.

The untreated Ni-B-Mo coated specimens with corrosion compounds are investigated using EDAX for chemical composition, which is presented in Figures 14 to 18. The EDAX results represent the peaks corresponding to the elements like Ni, B, Mo, C, O, Na and Cl on the corroded surfaces. The corrosion tests were conducted using the NaCl solution. Hence, the peaks of Na and Cl in the corrosion by-products may be correlated with the corrosive medium. The EDAX spectrum also contains peaks corresponding to C and O. The entire Nyquist plot contains a single semi-circular loop except the one presented in Figure 9a. The single loop confirms that the corrosive solution failed to penetrate through the coatings and reach the substrate. Hence, it can be concluded that the corrosion attack remained limited to the coated layer only. The EDAX tests are carried out using carbon tape, which may be the source of C in the EDAX result. The corrosion test findings and characterisation findings are aligned well with each other. Therefore, the Ni-B-Mo coated layer successfully prevented the corrosion attack to safeguard the steel substrate.

4. Conclusion

The untreated Ni-B-Mo coated specimens are developed at five different levels by varying the concentrations of three different parameters to analyse the impact of these parameters on corrosion resistance.

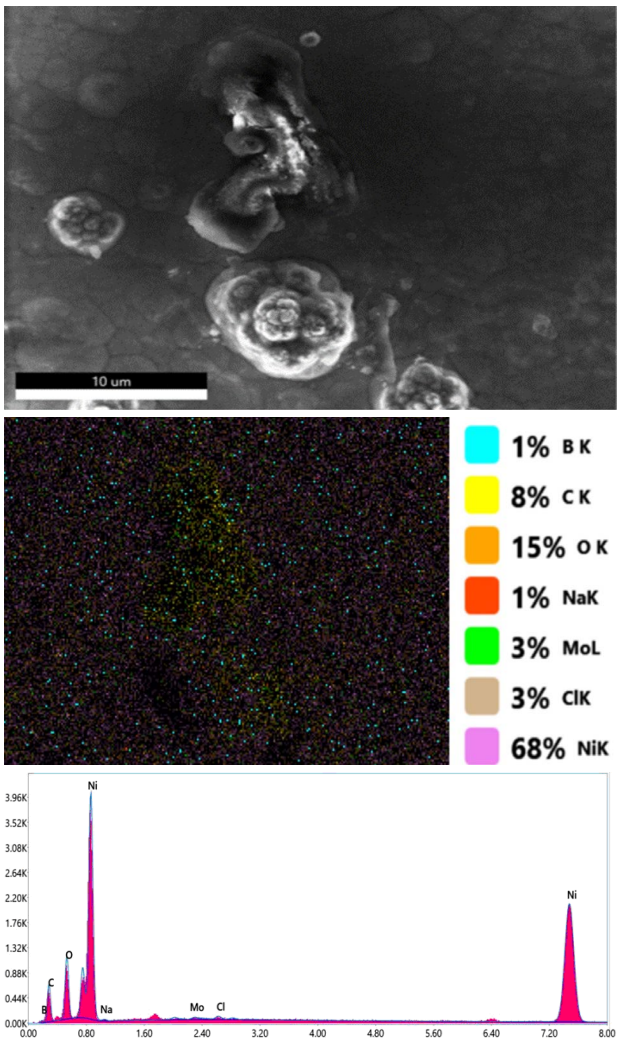

Figure 18. EDAX result of corroded surface obtained at bath concentration Level 5

The cross-cut coating thickness is improved from 13 to 42 µm with increased bath concentration level because of the acceleration in the chemical reaction process with higher borohydride concentration.

The untreated coated surfaces initially appear bright and then become darker with an increase in concentration level. They contain a uniform distribution of nodules to form morphology resembling cauliflower, which is very common in boron-based coatings.

The presence of boron increased from 3.70 to 6.50 wt. % while the molybdenum content also increased from 3.10 to 4.90 wt. %. Conversely, the nickel content decreased from 91.70 to 86.10 wt. %.

The coated specimens developed at Level 1 possess cracked surfaces. The inclusion of Mo in ENB coatings develops high stress, and increased concentration of $NaBH_4$ contributes to the development of a rougher surface due to accelerated chemical reaction. The *Ra* values range from 0.23 to 0.86 µm.

The corrosion resistance increases with the increase of $NaBH_4$ and Na_2MoO_4 concentrations up to their mid-level values, resulting in the best corrosion resistance behaviour at Level 3. The corrosion resistance declined with a further increase in concentrations of $NaBH_4$ and Na_2MoO_4 due to rougher surface formation and cracked morphology, respectively.

References

[1] F. Bülbül, H. Altun, V. Ezirmik, Ö. Küçük, Investigation of structural, tribological and corrosion properties of electroless Ni-B coating deposited on 316L stainless steel, Proceedings of the Institution of Mechanical Engineers, Part J: Journal of Engineering Tribology, Vol. 227, No. 6, 2013, pp. 629-639, DOI: 10.1177/1350650112464928

[2] Y. Wan, Y. Yu, L. Cao, M. Zhang, J. Gao, C. Qi, Corrosion and tribological performance of PTFE-coated electroless nickel boron coatings, Surface and Coatings Technology, Vol. 307, No. A, 2016, pp. 316-323, DOI: 10.1016/j.surfcoat.2016.09.001

[3] T. Miri, D. Seifzadeh, Z. Rajabalizadeh, Electroless Ni-B-MMT nanocomposite on magnesium alloy, Surface Engineering, Vol. 37, No. 9, 2021, pp. 1194-1205, DOI: 10.1080/02670844.2021.1959287

[4] P. Sahoo, S.K. Das, Tribology of electroless nickel coatings – A review, Materials & Design, Vol. 32, No. 4, 2011, pp. 1760-1775, DOI: 10.1016/j.matdes.2010.11.013

[5] M. Barman, T.K. Barman, P. Sahoo, Effect of borohydride concentration on tribological and mechanical behavior of electroless Ni-B coatings, Materials Research Express, Vol. 6, No. 12, 2019, Paper 126575, DOI: 10.1088/2053-1591/ab58b7

[6] S. Sürdem, C. Eseroğlu, R. Çitak, A parametric study on the relationship between $NaBH_4$ and tribological properties in the nickel-boron electroless depositions, Materials Research Express, Vol. 6, No. 12, 2019, Paper 125085, DOI: 10.1088/2053-1591/ab5beb

[7] S. Pal, N. Verma, V. Jayaram, S.K. Biswas, Y. Riddle, Characterization of phase transformation behaviour and microstructural development of electroless Ni-B coating, Materials Science and Engineering A, Vol. 528, No. 28, 2011, pp. 8269-8276, DOI: 10.1016/j.msea.2011.07.060

[8] M. Barman, T.K. Barman, P. Sahoo, Effect of heat-treatment temperature and borohydride concentration on corrosion behaviour of ENB

coating, Proceedings of the Institution of Mechanical Engineers, Part C: Journal of Mechanical Engineering Science, Vol. 237, No. 1, 2023, pp. 183-200, DOI: 10.1177/09544062221117677

[9] E. Correa, A.A. Zuleta, L. Guerra, M.A. Gómez, J.G. Castaño, F. Echeverría, H. Liu, P. Skeldon, G.E. Thompson, Tribological behavior of electroless Ni-B coatings on magnesium and AZ91D alloy, Wear, Vol. 305, No. 1-2, 2013, pp. 115-123, DOI: 10.1016/j.wear.2013.06.004

[10] J.N. Balaraju, A. Priyadarshi, V. Kumar, N.T. Manikandanath, P. Praveen Kumar, B. Ravisankar, Hardness and wear behaviour of electroless Ni-B coatings, Materials Science and Technology, Vol. 32, No. 16, 2016, pp. 1654-1665, DOI: 10.1080/02670836.2015.1137683

[11] V. Vitry, A. Sens, A.-F. Kanta, F. Delaunois, Experimental study on the formation and growth of electroless nickel-boron coatings from borohydride-reduced bath on mild steel, Applied Surface Science, Vol. 263, 2012, pp. 640-647, DOI: 10.1016/j.apsusc.2012.09.126

[12] R.A. Yildiz, K. Genel, T. Gulmez, Effect of heat treatments for electroless deposited Ni-B and Ni-W-B coatings on 7075 Al alloy, International Journal of Materials, Mechanics and Manufacturing, Vol. 5, No. 2, 2017, pp. 83-86, DOI: 10.18178/ijmmm.2017.5.2.295

[13] I.G. Serin, A. Göksenli, B. Yüksel, R.A. Yildiz, Effect of annealing temperature on the corrosion resistance of electroless Ni-B-Mo coatings, Journal of Materials Engineering and Performance, Vol. 24, No. 8, 2015, pp. 3032-3037, DOI: 10.1007/s11665-015-1568-0

[14] M.G. Hosseini, S. Ahmadiyeh, A. Rasooli, S. Khameneh-Asl, Pulse plating of Ni-W-B coating and study of its corrosion and wear resistance, Metallurgical and Materials Transactions A, Vol. 50, No. 11, 2019, pp. 5510-5524, DOI: 10.1007/s11661-019-05444-1

[15] V. Nemane, S. Chatterjee, Scratch and sliding wear testing of electroless Ni-B-W coating, Journal of Tribology, Vol. 142, No. 2, 2020, Paper 021705, DOI: 10.1115/1.4045165

[16] R.A. Yildiz, A. Göksenli, B.H. Yüksel, F. Muhaffel, A. Aydeniz, Effect of annealing temperature on the corrosion resistance of electroless produced Ni-B-W coatings, Advanced Materials Research, Vol. 651, 2013, pp. 263-268, DOI: 10.4028/www.scientific.net/AMR.651.263

[17] M. Barman, T.K. Barman, P. Sahoo, Corrosion behaviour of borohydride reduced Ni-B, Ni-B-W, Ni-B-Mo, Ni-B-W-Mo coatings with varying composition: A comparison, Journal of The Institution of Engineers (India): Series D, Vol. 105, No. 3, 2024, pp. 1733-1751, DOI: 10.1007/s40033-023-00574-8

[18] A.B. Radwan, R.A. Shakoor, A. Popelka, Improvement in properties of Ni-B coatings by the addition of mixed oxide nanoparticles, International Journal of Electrochemical Science, Vol. 10, No. 9, 2015, pp. 7548-7562, DOI: 10.1016/S1452-3981(23)17370-6

[19] V. Niksefat, M. Ghorbani, Mechanical and electrochemical properties of ultrasonic-assisted electroless deposition of Ni-B-TiO_2 composite coatings, Journal of Alloys and Compounds, Vol. 633, 2015, pp. 127-136, DOI: 10.1016/j.jallcom.2015.01.250

[20] H. Gul, İ. Usta, Effect of alumina concentration on morphology, wear, and corrosion: Electroless Ni-W-P/Al_2O_3 composite coatings on aluminum surfaces, Journal of Materials Engineering and Performance, Vol. 32, No. 13, 2023, pp. 6107-6122, DOI: 10.1007/s11665-023-08184-x

[21] H. Gül, The effect of TiO_2 concentration on morphology, wear and corrosion properties of NiB-TiO_2 composite coatings by ultrasonic-assisted pulse electrodeposition, Surface Topography: Metrology and Properties, Vol. 11, 2023, Paper 015001, DOI: 10.1088/2051-672X/acaff9

[22] R. Agrawal, L. Gupta, S. Jain, R. Sharma, A. Mukhopadhyay, Electroless Ni-B coating formed from a stabilizer-free double bath, Transactions of the Indian Institute of Metals, Vol. 77, No. 4, 2024, pp. 1039-1051, DOI: 10.1007/s12666-023-03220-9

[23] M. Köse, S. Tan, B. Yavuz, A.B. Demir, H. Algül, A.H. Kökçam, E.F. Erkan, M.F. Taşkin, H. Gül, Ö. Uygun, M. Uysal, A. Alp, Improving the tribological and corrosion behavior of Ni-B coating with low boron content from optimized lead-free bath on aluminum alloys, Surface and Coatings Technology, Vol. 494, No. 3, 2024, Paper 131464, DOI: 10.1016/j.surfcoat.2024.131464

[24] V. Vitry, J. Hastir, A. Mégret, S. Yazdani, M. Yunacti, L. Bonin, Recent advances in electroless nickel-boron coatings, Surface and Coatings Technology, Vol. 429, 2022, Paper 127937, DOI: 10.1016/j.surfcoat.2021.127937

[25] V. Vitry, L. Bonin, Increase of boron content in electroless nickel-boron coating by modification of plating conditions, Surface and Coatings Technology, Vol. 311, 2017, pp. 164-171, DOI: 10.1016/j.surfcoat.2017.01.009

[26] M. Barman, T.K. Barman, P. Sahoo, Tribo-mechanical behaviour of electroless Ni-B-Mo coatings with varying bath composition, Engineering Research Express, Vol. 5, No. 2, 2023, Paper 025072, DOI: 10.1088/2631-8695/acdd52

[27] V. Vitry, A. Sens, F. Delaunois, Comparison of various electroless nickel coatings on steel: Structure, hardness and abrasion resistance, Materials Science Forum, Vol. 783-786, 2014, pp. 1405-1413, DOI: 10.4028/www.scientific.net/MSF.783-786.1405

[28] J.N. Balaraju, N. Raman, N.T. Manikandanath, Nanocrystalline electroless nickel poly-alloy deposition: incorporation of W and Mo, Transactions of the IMF, Vol. 92, No. 3, 2014, pp. 169-176, DOI: 10.1179/0020296713Z.000000000123

[29] F. Madah, C. Dehghanian, A.A. Amadeh, Investigations on the wear mechanisms of electroless Ni-B coating during dry sliding and endurance life of the worn surfaces, Surface and Coatings Technology, Vol. 282, 2015, pp. 6-15, DOI: 10.1016/j.surfcoat.2015.09.003

[30] R. Agrawal, A. Mukhopadhyay, Development of Ni-B electroless coating from stabilizer free bath and characterization of high temperature tribological behaviour, scratch and corrosion resistance, Surface Topography: Metrology and Properties, Vol. 10, No. 4, 2022, Paper 045028, DOI: 10.1088/2051-672X/aca784

[31] V. Vitry, A.-F. Kanta, F. Delaunois, Application of nitriding to electroless nickel-boron coatings: Chemical and structural effects; mechanical characterization; corrosion resistance, Materials & Design, Vol. 39, 2012, pp. 269-278, DOI: 10.1016/j.matdes.2012.02.037

[32] A. Mukhopadhyay, T.K. Barman, P. Sahoo, Tribological behavior of electroless Ni-B-W coating at room and elevated temperatures, Proceedings of the Institution of Mechanical Engineers, Part J: Journal of Engineering Tribology, Vol. 232, No. 11, 2018, pp. 1450-1466, DOI: 10.1177/1350650118755781

[33] Q. Barati, S.M.M. Hadavi, Electroless Ni-B and composite coatings: A critical review on formation mechanism, properties, applications and future trends, Surfaces and Interfaces, Vol. 21, 2020, Paper 100702, DOI: 10.1016/j.surfin.2020.100702

[34] L. Bonin, C.C. Castro, V. Vitry, A.-L. Hantson, F. Delaunois, Optimization of electroless NiB deposition without stabilizer, based on surface roughness and plating rate, Journal of Alloys and Compounds, Vol. 767, 2018, pp. 276-284, DOI: 10.1016/j.jallcom.2018.06.330

[35] L. Bonin, V. Vitry, Mechanical and wear characterization of electroless nickel mono and bilayers and high boron-mid phosphorus electroless nickel duplex coatings, Surface and Coatings Technology, Vol. 307, No. A, 2016, pp. 957-962, DOI: 10.1016/j.surfcoat.2016.10.021

[36] M. Lekka, R. Offoiach, A. Lanzutti, M.Z. Mughal, M. Sebastiani, E. Bemporad, L. Fedrizzi, Ni-B electrodeposits with low B content: Effect of DMAB concentration on the internal stresses and the electrochemical behaviour, Surface and Coatings Technology, Vol. 344, 2018, pp. 190-196, DOI: 10.1016/j.surfcoat.2018.03.018

[37] D. Seifzadeh, H. Kazemi Mohsenabadia, Z. Rajabalizadeh, Electroless Ni-P plating on magnesium alloy by innovative, simple and non-toxic oxalate pretreatment and its corrosion protection, RSC Advances, Vol. 9, No. 99, 2016, pp. 97241-97252, DOI: 10.1039/C6RA19984D

[38] C. Domínguez-Ríos, A. Hurtado-Macias, R. Torres-Sánchez, M.A. Ramos, J. González-Hernández, Measurement of mechanical properties of an electroless Ni-B coating using nanoindentation, Industrial & Engineering Chemistry Research, Vol. 51, No. 22, 2012, pp. 7762-7768, DOI: 10.1021/ie201760g

[39] E. Georgiza, V. Gouda, P. Vassiliou, Production and properties of composite electroless Ni-B-SiC coatings, Surface and Coatings Technology, Vol. 325, 2017, pp. 46-51, DOI: 10.1016/j.surfcoat.2017.06.019

[40] S. Yazdani, F. Mahboubi, Comparison between microstructure, wear behavior, and corrosion resistance of plasma-nitrided and vacuum heat-treated electroless Ni-B coating, Journal of Bio- and Tribo-Corrosion, Vol. 5, No. 3, 2019, Paper 69, DOI: 10.1007/s40735-019-0264-2